Chemical Engineering Journal 523 (2025) 168910

Contents lists available at ScienceDirect

Chemical Engineering Journal

journal homepage: www.elsevier.com/locate/cej

Solvent-driven phase separation strategy for eco-friendly high-performance organic gas sensors

Seong Jin Kim [a], Duho Jang [a], Soyeon An [c], Dong-Ku Kang [c], Yeong Don Park [a,b,*]

[a] Department of Energy and Chemical Engineering, Incheon National University, Incheon, 22012, Republic of Korea
[b] Innovation Center for Chemical Engineering, Incheon National University, Incheon, 22012, Republic of Korea
[c] Department of Chemistry, Incheon National University, Incheon, 22012, Republic of Korea

ARTICLE INFO

Keywords:
Biodegradable polymer
Organic gas sensors
Phase separation
OFET
P3HT

ABSTRACT

Organic electronic devices offer several advantages over conventional inorganic materials, such as flexibility, light weight, and low cost; however, their poor stability in atmospheric environments remains a significant limitation. The increasing environmental pollution caused by organic electronic waste has led to a growing interest in biodegradable polymers as sustainable alternatives. This study presents the development of an eco-friendly organic gas sensor based on blended films of poly(3-hexylthiophene) (P3HT) and poly(butylene succinate) (PBS). The organic transistor maintained a stable device performance even with up to 90 wt% reduction in P3HT content through vertical phase separation via slow evaporation of the high-boiling-point solvent, dichlorobenzene (DCB). Notably, the chloroform (CF)-processed films exhibited horizontal phase separation, which enhanced their gas-sensing performance owing to the presence of gas-ester groups in PBS in the active layer. Furthermore, the intrinsic flexibility of PBS improved the mechanical durability of the active layer, which was shown to be biodegradable in seawater. This study demonstrates that solvent engineering is a powerful strategy for optimizing the multifunctional properties of polymer blends, thereby providing an environmentally sustainable and highly sensitive gas-sensing platform.

1. Introduction

The rapid expansion of industrialization has led to a sharp increase in the demand for highly sensitive and selective gas sensors capable of detecting hazardous air pollutants such as oxidizing gas, and volatile organic compounds (VOCs) [1–3]. Among these pollutants, nitrogen dioxide (NO_2), predominantly generated from fossil fuel combustion, poses a serious threat to human health, causing respiratory illnesses including pulmonary edema, bronchitis, and asthma [2–4]. Therefore, the development of portable gas sensors with high sensitivity, selectivity, and long-term operational stability is essential for the effective real-time monitoring oxidizing gas [5,6].

To date, various gas sensing technologies have been explored, including gas chromatography sensors, electrochemical sensors, optical sensors, and semiconductor-based sensors [7–9]. Semiconductor-based resistive and capacitive sensors are widely utilized owing to their straightforward architecture, low energy requirements and rapid response characteristics [8,10–12]. Field-effect transistor-type gas sensors have emerged as a promising platform due to their superior gas sensing performance caused by their unique signal amplification capabilities [13–16]. In particular, organic field-effect transistor (OFET)-based gas sensors are suitable for high sensitive portable gas sensors due to their lightweight, flexibility, and simple fabrication processes [14,15,17].

The gas sensing mechanism of OFETs relies on charge transfer or electronic doping at the interface between the analyte gases and the organic semiconductor layer [15,18–20]. However, the charge conduction channel in OFETs is confined to only a few nanometers near the dielectric interface [21], limiting gas molecule diffusion into the active layer. A further critical challenge is the limited lifetime of organic semiconductors by moisture or oxygen [22,23], which leads to degradation in device performance over time, resulting in the accumulation of electronic waste [24,25]. The conventional method is the encapsulation film coating to prevent oxygen, moisture, and light diffusion into the organic active layer [26], but gas sensors that must be exposed to external gas are difficult to encapsulate active layer [19,20]. Thus, the development of sustainable alternatives is urgently required to minimize polymer waste. Biodegradable polymers have attracted increasing

* Corresponding author at: Department of Energy and Chemical Engineering, Incheon National University, Incheon, 22012, Republic of Korea.
E-mail address: ydpark@inu.ac.kr (Y.D. Park).

https://doi.org/10.1016/j.cej.2025.168910
Received 7 July 2025; Received in revised form 26 August 2025; Accepted 24 September 2025
Available online 24 September 2025

attention as environmentally friendly materials capable of decomposing into non-toxic byproducts via enzymatic or hydrolytic degradation [27–29]. Unlike conventional synthetic polymers that do not degrade in the atmosphere environment for decades, biodegradable polymers offer a more sustainable pathway [27,30].

In this study, we developed an eco-friendly organic gas sensor introducing a biodegradable polymer, poly(butylene succinate) (PBS) into the active layer of poly(3-hexylthiophene) (P3HT). PBS can be efficiently degraded in both marine and soil environments, supporting its potential to reduce electronic waste. Solvents with different boiling points were used to induce effective horizontal and vertical phase separation of conjugated polymers and biodegradable polymers. When the active layer was vertically separated, a P3HT-rich network on the upper surface maintained stable device performance even at very low P3HT content due to efficient charge transport. Mechanical stretching tests further confirm that the intrinsic flexibility of PBS improves the mechanical durability of the blending film. Additionally, the active layer in gas sensor exhibited clear signs of biodegradation in seawater, demonstrating their potential as environmentally friendly gas sensing materials. We believe that this work presents a sustainable strategy for the development of eco-friendly organic gas sensors by integrating biodegradable polymers, simultaneously addressing device performance and environmental impact.

2. Experimental details

2.1. Fabrication of OFETs and gas sensors

P3HT (Mw = 58 kDa, regioregularity = 96 %, 2.0 ≤ PDI ≤ 2.3) was purchased from Rieke Metals and used as a p-type semiconducting material without further purification. PBS (BG 5000 J) was purchased from ANKOR Bioplastics. Blend solutions of P3HT and PBS with varying weight ratios were prepared at a concentration of 5 mg mL^{-1} in CF or a 9:1 *v*/v mixture of chloroform and dichlorobenzene (CF:DCB). The P3HT/PBS blend solution was subjected to magnetic stirring at 750 rpm on a hotplate at 45 °C for 2 h to achieve complete dissolution, and was subsequently allowed to cool to room temperature over 1 h.

A highly doped n-type silicon wafer with a 3000 Å thick silicon dioxide (SiO_2) layer was cleaned using a piranha solution to remove organic contaminants. The P3HT/PBS blend solutions were spin-coated onto cleaned SiO_2/Si substrates at 1500 rpm for 60 s to form uniform films. Bottom-gate top-contact OFET devices were fabricated by thermally evaporating gold (Au) electrodes. A shadow mask with a square pattern, featuring a channel length of 100 μm and a channel width of 2000 μm, was used for the deposition of Au source and drain electrodes in OFET-based gas sensors. For UV–Vis absorption measurements, P3HT/PBS films were prepared on cleaned quartz substrates following the same spin-coating process used for the silicon substrates.

2.2. Characterization

The molecular order of the P3HT films was examined by measuring the UV–Vis absorption spectra using a UV–Vis spectrophotometer (Lambda 365, PerkinElmer). The surface morphologies of the P3HT/PBS blended films were analyzed using optical microscopy (OM, BX51). The contact angles of deionized (DI) water and diiodomethane (CH_2I_2) were measured using a contact angle meter (Phoenix-MT, M.A.T, S.E.O. Co.) to evaluate the surface energy and phase separation behavior of the films. In addition, X-ray photoelectron spectroscopy (XPS, NEXSA G2) was employed to analyze the elemental composition of the film surfaces and investigate the phase separation of the films.

The electrical characteristics of the OFET devices were evaluated under ambient and vacuum conditions using a semiconductor parameter analyzer (Keithley 4200-SCS) to determine their charge-transport properties and field-effect mobility. Additionally, the gas sensing performance of the OFET-based sensors was assessed at room temperature using a gas sensor testing system (GASENTEST), with the gate voltage (V_G) and drain voltage (V_D) set to −10 V. Measurements were recorded using a semiconductor analyzer (Keithley 2636B). In the pulse-cycle sensing test, the gas concentration was maintained at 10 ppm, whereas in the dynamic-cycle test, the gas concentration was varied from 10 to 100 ppm. Under all experimental conditions, gas was supplied from calibrated gas cylinders containing an air mixture.

For the film-stretching test, Ecoflex substrates were fabricated by mixing Ecoflex resin and a curing agent (Ecoflex, 00–20) in a 1:1 volume ratio, allowing the mixture to cure at room temperature. To obtain freestanding films, P3HT/PBS blend films, initially coated on SiO_2/Si substrates, were immersed in a hydrofluoric acid (HF, ACS reagent, 48 %) solution to etch the underlying SiO_2 layer. The released films were then carefully transferred onto Ecoflex substrates. Uniaxial tensile strains of 0 %, 30 %, 50 %, 70 %, and 100 % were applied using a tensile manipulator (BM100, ECOPIA), and the morphological changes in the stretched films were subsequently characterized by OM. For the evaluation of bending durability, flexible polyethylene terephthalate (PET) substrates were used. Bending durability was evaluated at a fixed radius of 5 mm for 100, 500, 1000, 3000, and 5000 cycles. After each cycle set, the charge-transport properties were measured.

For the biodegradation test, natural seawater from the Yellow Sea (Incheon, South Korea) was dropped onto the P3HT:PBS blend films until the surface was fully covered. Morphological changes upon seawater exposure were monitored over time using OM. The same fabrication process used for the stretching test was employed for the biodegradation test in the bottom region of the blended film. P3HT/PBS blend films were spin-coated onto SiO_2/Si substrates and subsequently immersed in HF to etch the SiO_2 layer. The detached films were then transferred onto Ecoflex substrates, and the original top and bottom layers were reversed.

3. Results and discussion

3.1. Phase separation of P3HT/PBS blend films

The optical properties of the P3HT/PBS blend films were examined using UV–Vis absorption spectroscopy. Pristine P3HT films had thicknesses of approximately 60–70 nm regardless of solvent type as determined by UV–Vis absorption analysis. UV–Vis spectroscopy revealed that pristine P3HT showed distinct vibronic peaks ((0–0), (0–1), (0–2)) associated with π–π interactions [31,32], while PBS displayed no absorption at wavelength in the 200 nm ~ 800 nm range (Fig. 1). Increasing the PBS content led to an overall decrease in the peak intensity due to the dilution effect and the absence of PBS absorption features (Figs. 1a and c). In CF-processed films, the A_{0-0}/A_{0-1} ratio decreased with increasing PBS content, indicating disrupted π–π stacking of P3HT molecules (Figs. 1b and S1) [33]. In contrast, CF:DCB-processed films maintained the A_{0-0}/A_{0-1} ratio, suggesting improved π–π stacking of P3HT chains as a result of vertical phase separation (Fig. 1d) [33,34].

To investigate solvent-dependent morphological differences [35–37], P3HT/PBS blend films processed with CF and CF:DCB with PBS contents were investigated using OM. CF-processed films exhibited pronounced lateral phase separation, resulting in heterogeneous surface morphologies. In contrast, CF:DCB-processed films displayed uniform surface textures across all compositions, indicating vertical phase separation (Fig. 1e). The phase separation behavior is further elucidated schematically in Fig. 1f. In CF-processed films, rapid solvent evaporation driven by the low boiling point of CF (61.2 °C) limited polymer chain rearrangement time [35–38], leading to lateral (horizontal) phase separation, [39–41] where P3HT-rich and PBS-rich domains coexist side by side. In contrast, the addition of high-boiling-point DCB (180.5 °C) slowed solvent evaporation [35,37,42], thereby allowing sufficient time for vertical phase separation [42,43]. Consequently, PBS, with a relatively high surface energy owing to its ester functional group, shifted

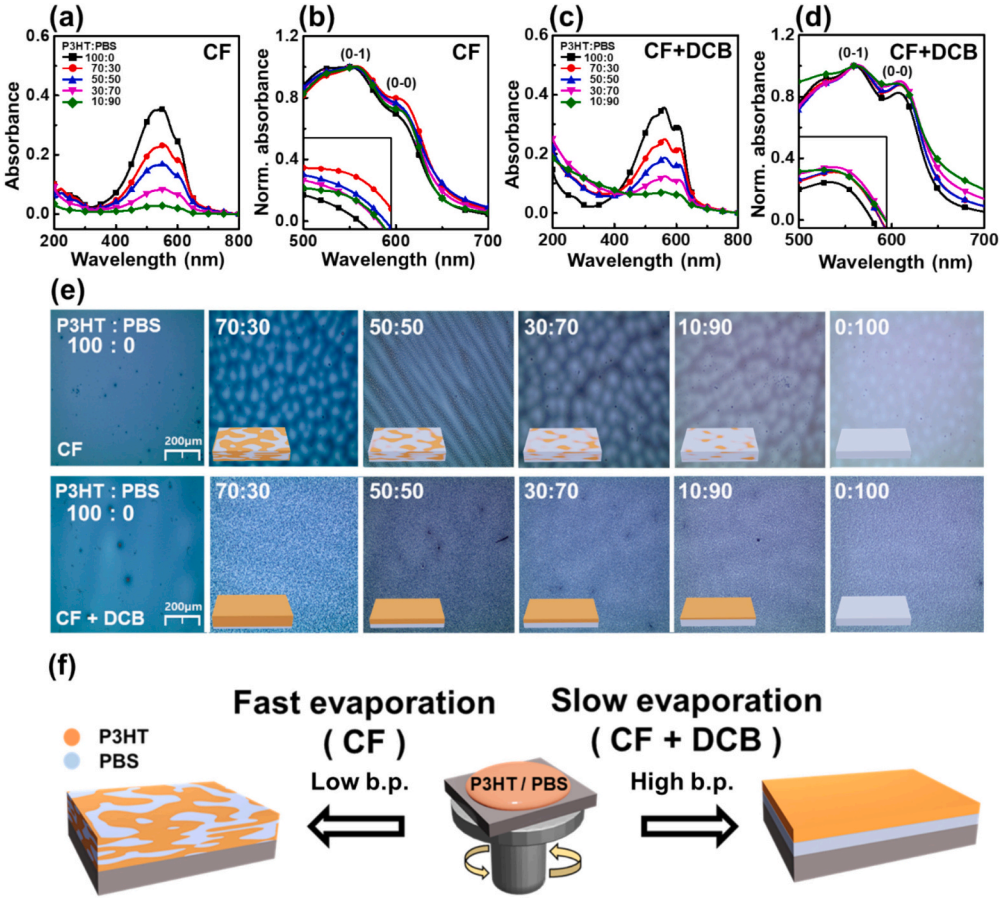

Fig. 1. UV–Vis absorption spectra of P3HT/PBS blend films processed with (a) CF and (c) CF:DCB (9:1, *v*/v%) with PBS contents. Normalized UV–Vis absorption spectra of P3HT/PBS blend films processed with (b) CF and (d) CF:DCB. (e) OM images of P3HT/PBS blend films processed with CF and CF:DCB with PBS contents. (f) Schematic illustration of the phase separation mechanism of the active layer depending on the solvent systems.

preferentially toward the bottom of the film, whereas P3HT, with lower surface energy, was located on the upper air surface [44,45], indicating a uniform film morphology. These findings emphasize the critical role of solvent engineering in modulating phase separation pathways and microstructural organization in P3HT/PBS blend films.

To confirm the phase separation behavior, the surface wettability of the P3HT/PBS blend films with varying PBS contents was investigated using water contact angle measurements (Fig. 2). In CF-processed blend films, the contact angle decreased with increasing PBS content, which was attributed to horizontal phase separation driven by the rapid evaporation of the low-boiling-point CF solvent. In contrast, for the blend films processed with the CF:DCB mixed solvent, the contact angles remained relatively constant, regardless of the PBS content (Figs. 2a and b). These results indicate that DCB, with a high boiling point, slowed the solidification rate and induced vertical phase separation of the polymers (Fig. 2c). The different trends in contact angle changes with the PBS content can be rationalized by the surface energy difference between P3HT and PBS [46–48]. The surface energies of P3HT and PBS were calculated using Eq. (1) based on measurements with DI water and CH_2I_2 (Fig. S2 and Table S1) [49].

$$(1+\cos(\theta))\gamma_{LV} = 2\sqrt{\gamma_S^D+\gamma_L^D}+2\sqrt{\gamma_S^P+\gamma_L^P} \quad (1)$$

As PBS (55.2 mN m^{-1}) has higher surface energy than P3HT owing to its ester functional groups (41.4 mN m^{-1}), it is located close to hydrophilic SiO_2 substrate than the air surface. Therefore, vertical phase separation between the two polymers with different surface energies was induced by the slow solvent evaporation of DCB. These findings highlight the pivotal role of solvent engineering in controlling phase separation behavior in conjugated polymer blend systems, which is critical for optimizing device performance in organic electronic applications.

3.2. Chemical composition of P3HT/PBS blend films

To elucidate the vertical phase separation behavior of P3HT/PBS blend films, the elemental compositions of the top and bottom surfaces of blend films processed with CF and CF:DCB solvents were determined using XPS (Fig. 3). In the C1s spectra, CF-processed blend films exhibited prominent C—O (~286.1 eV) and O=C–O (~288.5 eV) peaks at both the top and bottom surfaces (Fig. 3a) [50,51]. This indicated a relatively uniform distribution of PBS with oxygen-containing functional groups, suggesting lateral phase separation between P3HT and PBS. In contrast, the CF:DCB-processed blend films showed strong C–C/C–H peaks (~284.8 eV) with negligible C—O and O=C–O contributions at the top surface [52], while signals corresponding to oxygen-containing species were present at the bottom surface (Fig. 3b). The S2p spectra further support this conclusion. For CF-process blend films, sulfur signals associated with the thiophene rings of P3HT were observed on both surfaces [52], reflecting a mixed distribution (Fig. 3b). However, in the CF: DCB-processed blend films, the S2p signal was intense at the top surface and nearly disappeared at the bottom, further confirming vertical segregation phase separation of P3HT:PBS films (Fig. 3e). The CF-processed P3HT/PBS blend films exhibited similar O1s peak intensities at both the top and bottom surfaces (Fig. 3c), whereas the CF:DCB-processed P3HT/PBS blend films showed a markedly stronger O1s peak at the bottom surface (Fig. 3f). These findings clearly support a vertically phase-separated morphology, where P3HT is enriched at the

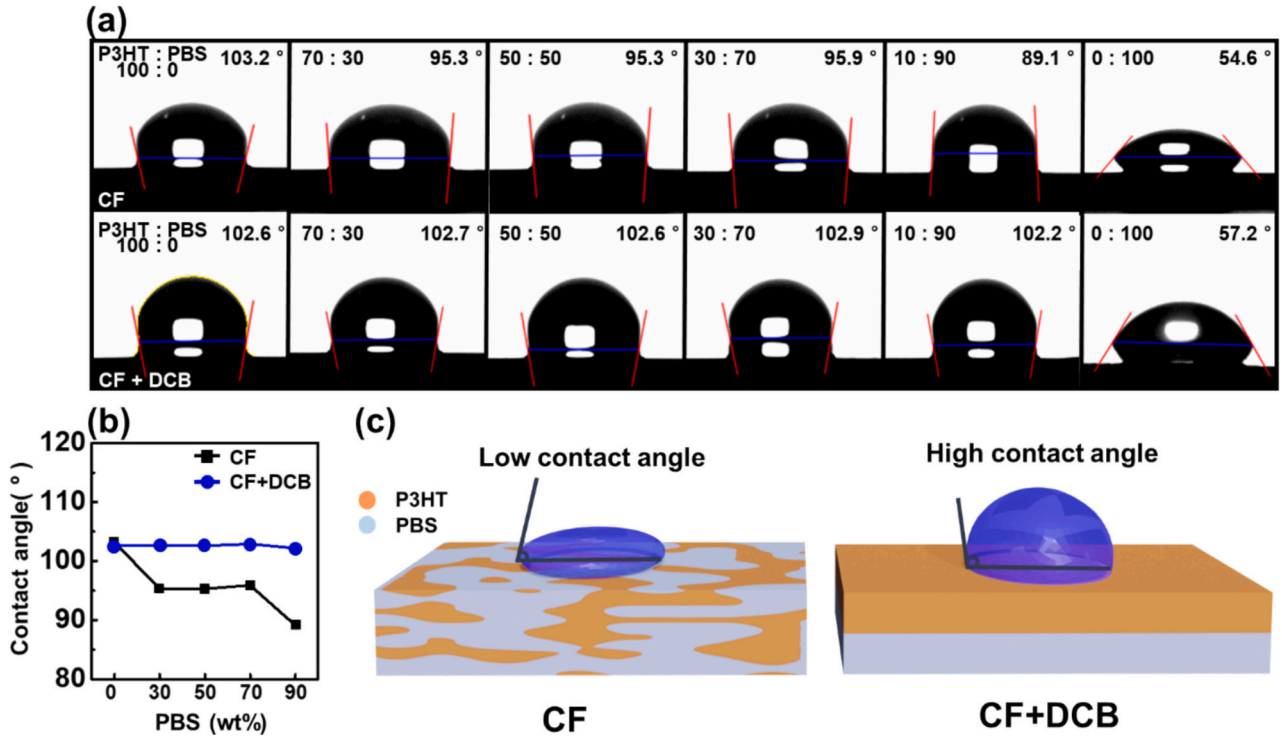

Fig. 2. (a) Water contact angle of P3HT/PBS blend films processed with CF and CF:DCB with PBS contents. (b) Contact angle variation graph of P3HT/PBS blend films as a function of PBS content for CF and CF:DCB. (c) Schematic illustration of the water contact angle of the active layer processed with CF and CF:DCB.

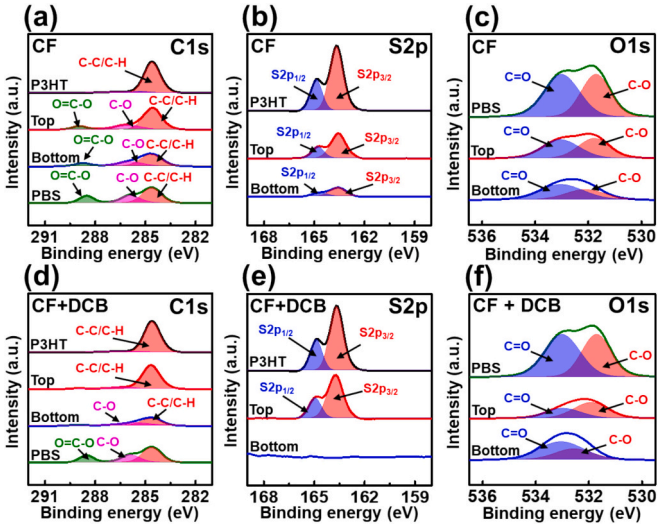

Fig. 3. XPS spectra of (a) C1s, (b) S2p and (c) O1s in P3HT:PBS (50:50 wt%) blend films processed with CF, (d) C1s, (e) S2p and (f) O1s in P3HT:PBS (50:50 wt%) blend films processed with CF:DCB.

air/film interface and PBS is segregated toward the substrate, owing to their surface energy differences [44]. The high volatility of CF led to lateral random mixing, whereas the slow evaporation of DCB promoted vertical phase separation between the P3HT and PBS layers. These findings highlight the pivotal role of solvent engineering in controlling the phase separation behavior of conjugated polymer blend systems, which is critical for optimizing the device performance in organic electronic applications.

3.3. Charge transport and gas sensing performance

The electrical properties of the OFETs based on the P3HT/PBS blend films were evaluated in terms of solvent composition and PBS content (Fig. 4). For the P3HT/PBS blend films processed with CF, the field-effect mobility and on-off ratio gradually decreased as the PBS content increased, and the OFET ceased to function when the PBS content exceeded 50 wt%. (Figs. 4a and b). These results are attributed to the horizontal phase separation of the CF-processed films, where the insulating PBS domains disrupt the charge transport and induce charge trapping. Ester functional group in PBS domains can act as charge traps at the semiconductor–insulator interface, capturing and releasing carriers during device operation, thereby altering the threshold voltage and reducing the drain currents (Fig. 4c) [53–55]. In contrast, although the field-effect mobility and on-off ratio of the P3HT:PBS films processed with CF:DCB decreased with increasing PBS content, their electrical performance was retained even when the P3HT content was reduced to 10 wt% (Figs. 4d and e). This is attributed to the vertically phase-separated active layer, where the P3HT-rich top layer maintains continuous charge-transport pathways [35,43,56,57]. The high boiling point of DCB promoted vertical separation in the active layer by slowing solvent evaporation and enhancing molecular order, thereby supporting efficient charge transport even at high PBS contents (Fig. 4f).

Dynamic responses of P3HT/PBS blend films were recorded under exposure to NO_2, SO_2, and CO_2 at concentrations of 10–100 ppm (Fig. 5). The responsivity ($\Delta I_D/I_0$), response rate ($\Delta R/\Delta t$), and recovery rate ($\Delta R/\Delta t$) were calculated from the responses ($-\Delta I_D/I_0$) under 10 ppm NO_2 gas exposure (Fig. S3). As the PBS content increased, the sensing performances of both devices improved owing to the presence of ester functional groups in PBS. Notably, the CF-only processed P3HT/PBS blend films exhibited superior sensing characteristics compared to their CF:DCB-processed counterparts (Figs. 5a–d). This enhancement is attributed to lateral phase-separated morphologies formed by the rapid evaporation of CF, which induce ester-functional group of PBS close to the surface, thereby facilitating NO_2 adsorption (Fig. 5m) [29,58]. In

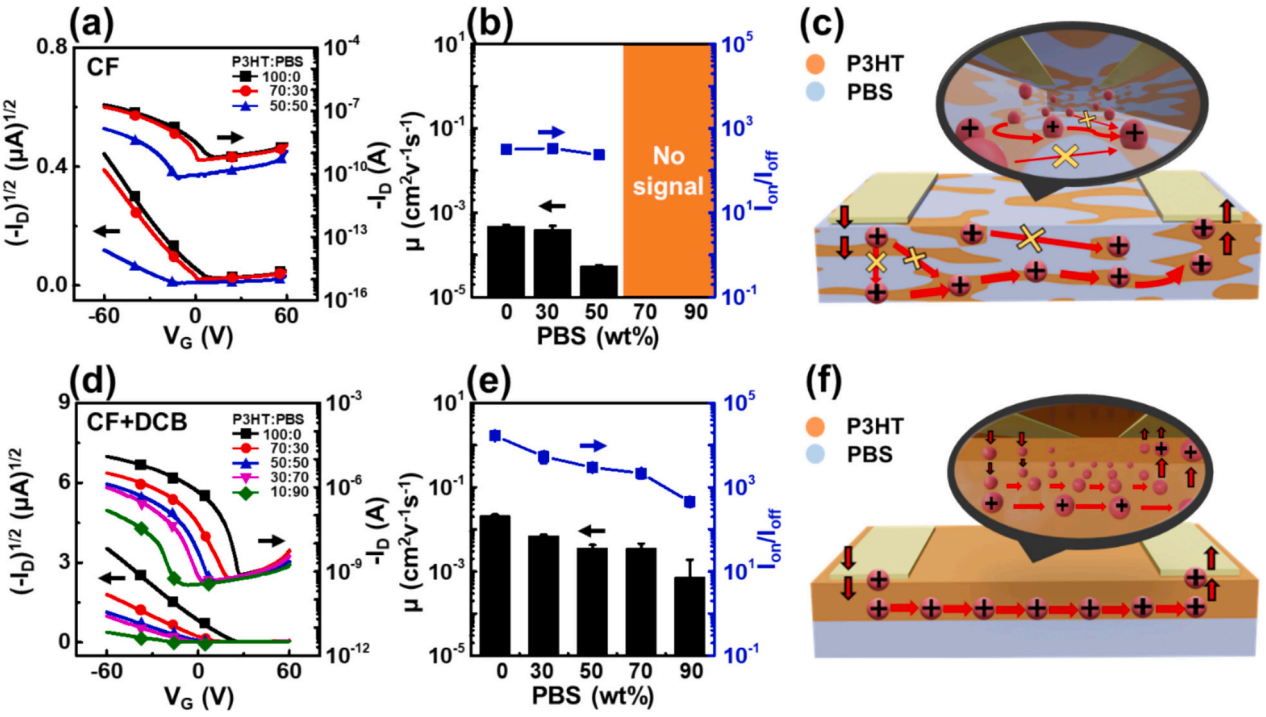

Fig. 4. Charge transport characteristics of P3HT/PBS blend films processed with (a) CF and (d) CF:DCB varying PBS content in different solvent systems. Change of field-effect mobility (left axis) and turn-on/off current ratio (right axis) of P3HT/PBS blend films processed with (b) CF and (e) CF:DCB with PBS content. Schematic illustrations of charge transport mechanisms in P3HT/PBS blend films processed with (c) CF and (f) CF:DCB.

contrast, the slow evaporation rate of DCB promotes vertical phase separation in CF:DCB-processed P3HT/PBS blend films. Although the overall sensing performance was slightly reduced, the CF:DCB-processed films still exhibited excellent gas sensitivity, even with only 10 % P3HT content, owing to the formation of a continuous P3HT network facilitated by the vertical phase-separated morphology (Fig. 5n).

The dynamic responses to SO_2 and CO_2 were also evaluated (Figs. 5e–h). All devices exhibited measurable yet notably weaker responses to SO_2, particularly at higher PBS concentrations. In the case of CO_2, the response was minimal, regardless of the processing conditions, reflecting its inherently low reactivity with the sensing layer. These trends were further corroborated by a signal trend analysis (Fig. S4). Compared to NO_2, both SO_2 and CO_2 yielded significantly lower sensitivities and higher limit of detection (LOD) values across all compositions and solvent systems (Figs. 5i–l) [59,60]. This pronounced selectivity toward NO_2 is attributed to its strong oxidizing properties and high electron affinity [60–62], which facilitate more efficient charge transfer at the active layer. Accordingly, the P3HT/PBS blend sensors demonstrated clear gas discrimination capability, with a distinct preference for NO_2 over SO_2 and CO_2 [63].

The sensitivities and LOD values clearly highlight the distinct gas-sensing behaviors of the two solvent systems. In particular, the CF-processed device containing 50 wt% PBS exhibited the lowest LOD of 4.65×10^{-2} ppm for NO_2, whereas its CF:DCB-processed counterpart showed a significantly higher LOD of 2.62×10^{-1} ppm for NO_2 (Tables 1 and 2). Notably, even at a high PBS content of 90 wt%, the CF:DCB-processed device maintained a relatively low LOD of 7.36×10^{-2} ppm for NO_2, suggesting that vertical phase separation can effectively preserve NO_2 sensing performance despite substantial reduction in P3HT content (Table S2) [64–67].

The gas-sensing behavior of the P3HT/PBS blend films is significantly governed by the choice of solvent, which dictates phase-separation morphology and spatial distribution of the sensing-active PBS domains. Processing with CF induces lateral phase separation, enriching PBS at the surface and thereby enhancing NO_2 adsorption and sensitivity. In contrast, the CF:DCB processing promoted vertical phase separation, enabling sustained sensing performance even at high PBS content owing to the formation of a continuous P3HT network. Under all tested conditions, the sensors exhibited the highest selectivity and sensitivity toward NO_2, attributed to its high electron affinity, thereby underscoring the importance of morphological control in engineering high-performance polymer-based gas sensors.

We examined the effect of relative humidity (RH 20 %, 40 %, and 60 %) on the NO_2 sensing performance of P3HT/PBS blend films processed using two different solvent systems (CF and CF:DCB) (Fig. S5). The NO_2 sensitivity gradually decreased with humidity, which can be attributed to the strong interaction between the ester groups of PBS and water molecules, thereby suppressing NO_2 adsorption in the sensing layer. This humidity-induced inhibition of NO_2 adsorption was more pronounced in the P3HT/PBS blend films than in the pristine P3HT films. In particular, for the CF-processed films, the horizontally phase-separated structure resulted in greater exposure of PBS domains to moisture, which enhanced water adsorption and consequently made NO_2 adsorption more difficult, leading to a more significant reduction in sensitivity under humid conditions.

3.4. *Mechanical properties of P3HT/PBS blend films*

A key advantage of organic electronic devices is their flexibility, which is largely determined by their crystallinity and intrinsic properties [18,30,69]. Stretching tests were conducted to assess the mechanical characteristics of P3HT/PBS blend films with different PBS ratios. The stretching test was based on the optimal P3HT/PBS composition for transistor operation in each solvent system. The P3HT/PBS blended films were subjected to tensile strain, and their morphologies were examined using OM. The P3HT/PBS blended film was transferred onto an Ecoflex substrate for stretching analysis (Fig. 6a) [37,68]. Owing to the inverted transfer process, the OM images primarily show the bottom region of the active layer. For CF-processed films, homo P3HT exhibited large cracks at 50 % deformation, demonstrating less flexible properties.

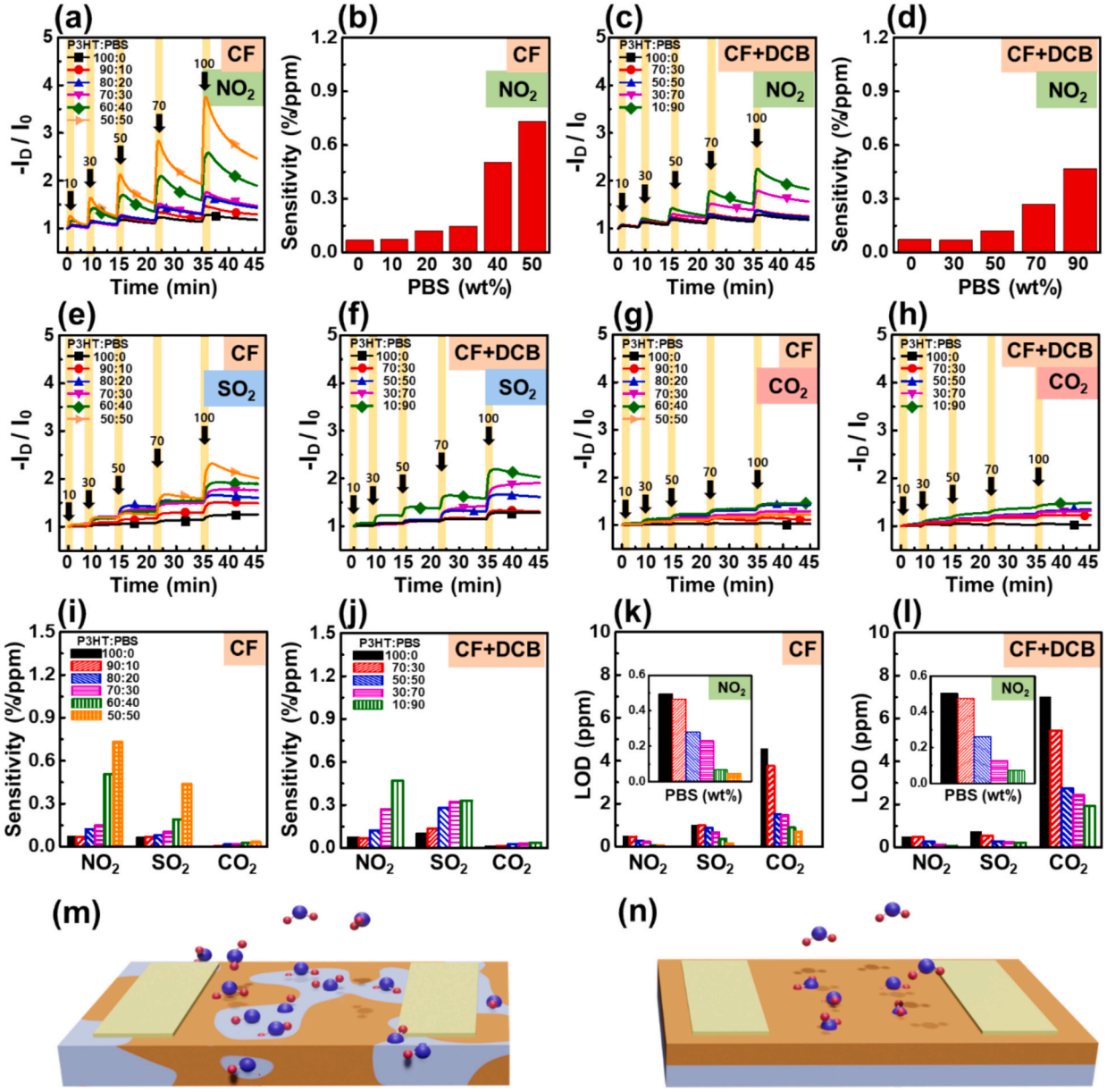

Fig. 5. Dynamic responses to NO_2 for P3HT/PBS films processed with (a) CF and (c) CF:DCB. The corresponding sensitivities to NO_2 for films processed with (b) CF and (d) CF:DCB. Dynamic responses to SO_2 for P3HT/PBS films processed with (e) CF and (f) CF:DCB, and to CO_2 for P3HT/PBS films processed with (g) CF and (h) CF:DCB. Sensitivity for various gases in P3HT/PBS films processed with (i) CF and (j) CF:DCB. LOD for the various gases in P3HT/PBS films processed with (k) CF and (l) CF:DCB. Insets highlight magnified LOD values for NO_2. Schematic illustrations of adsorption behavior of gas sensor processed with (m) CF and (n) CF:DCB.

Table 1
Sensitivity and LOD of P3HT/PBS blend films processed with CF for NO_2.

P3HT : PBS (wt%)	Sensitivity (%/ppm)	LOD (ppm)
100 : 0	6.88×10^{-2}	4.94×10^{-1}
90 : 10	7.30×10^{-2}	4.66×10^{-1}
80 : 20	1.22×10^{-1}	2.79×10^{-1}
70 : 30	1.47×10^{-1}	2.31×10^{-1}
60 : 40	5.05×10^{-1}	6.73×10^{-2}
50 : 50	7.31×10^{-1}	4.65×10^{-2}

Table 2
Sensitivity and LOD of P3HT/PBS blend films processed with CF:DCB for NO_2.

P3HT : PBS (wt%)	Sensitivity (%/ppm)	LOD (ppm)
100 : 0	7.30×10^{-2}	5.03×10^{-1}
70 : 30	6.88×10^{-2}	4.74×10^{-1}
50 : 50	1.22×10^{-1}	2.62×10^{-1}
30 : 70	2.70×10^{-1}	1.28×10^{-1}
10 : 90	4.70×10^{-1}	7.36×10^{-2}

However, large cracks were not observed in the P3HT/PBS film containing 50 wt% PBS, indicating improved mechanical flexibility (Fig. 6b). PBS, with a low glass transition temperature, provides inherent flexibility that enhances the mechanical properties of the blend film with horizontal phase separation, allowing it to withstand strong deformations.

Of CF:DCB-processed films, the P3HT film showed large cracks at 30 % strain because of increased crystallinity induced by the DCB solvent [37]. However, the crack formation was significantly suppressed with increasing PBS content, indicating excellent mechanical robustness (Fig. 6c). This improvement in flexibility can be explained by solvent-

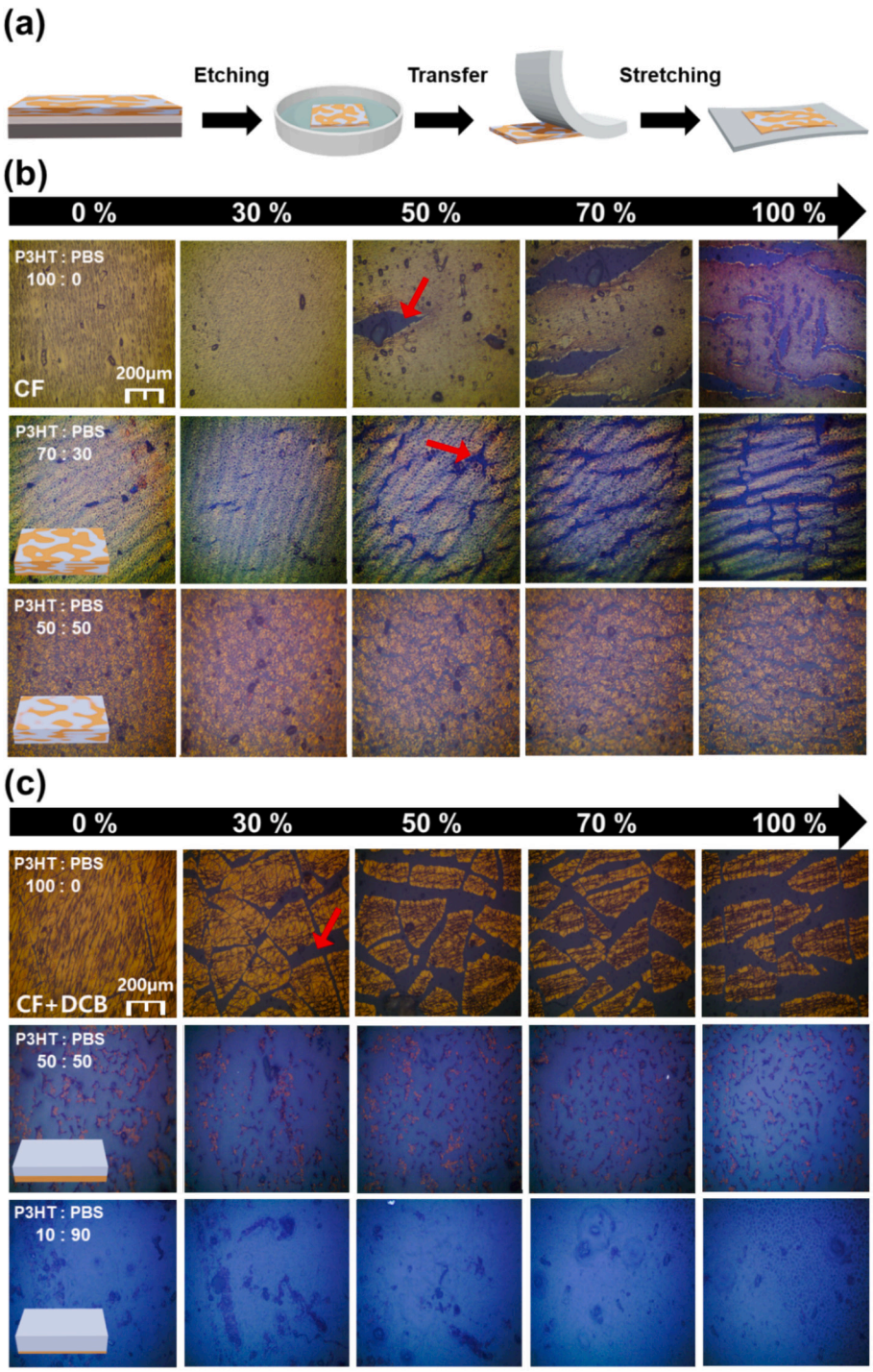

Fig. 6. (a) Schematic illustration of the stretching test for P3HT/PBS blend films transferred onto Ecoflex substrates. OM images showing the morphology of P3HT/PBS blend films processed with (b) CF and (c) CF:DCB under different stretching strains.

induced vertical phase separation, where the bottom region of the active layer is primarily composed of PBS. The elastic PBS layer acts as a stress-buffering interface [70,71], effectively alleviating mechanical strain in the P3HT layer. These results highlight the critical role of phase separation control and solvent processing strategies in optimizing the mechanical durability of films for flexible organic electronic applications. P3HT/PBS blend films with higher PBS content exhibited smaller reductions in field-effect mobility, due to the flexibility of PBS (Fig. S6). These results confirm that PBS incorporation contribute critically to enhancing the mechanical stability of the OFETs. Especially in CF:DCB-processed films, pristine P3HT has more crystalline phase resulting in less flexibility. The field-effect mobility of pristine P3HT was decreased by more than two order after bending test, but P3HT films with 90 wt% PBS was maintained field-effect mobility and showed excellent bending stability.

3.5. *Bio-degradation of P3HT/PBS blend films*

To evaluate the degradability of the active layers, seawater droplets were applied to the surface of the P3HT/PBS blend films, and morphological changes were monitored over time using OM (Fig. 7) [28,29,72]. The P3HT/PBS blend films processed with CF exhibited horizontal phase

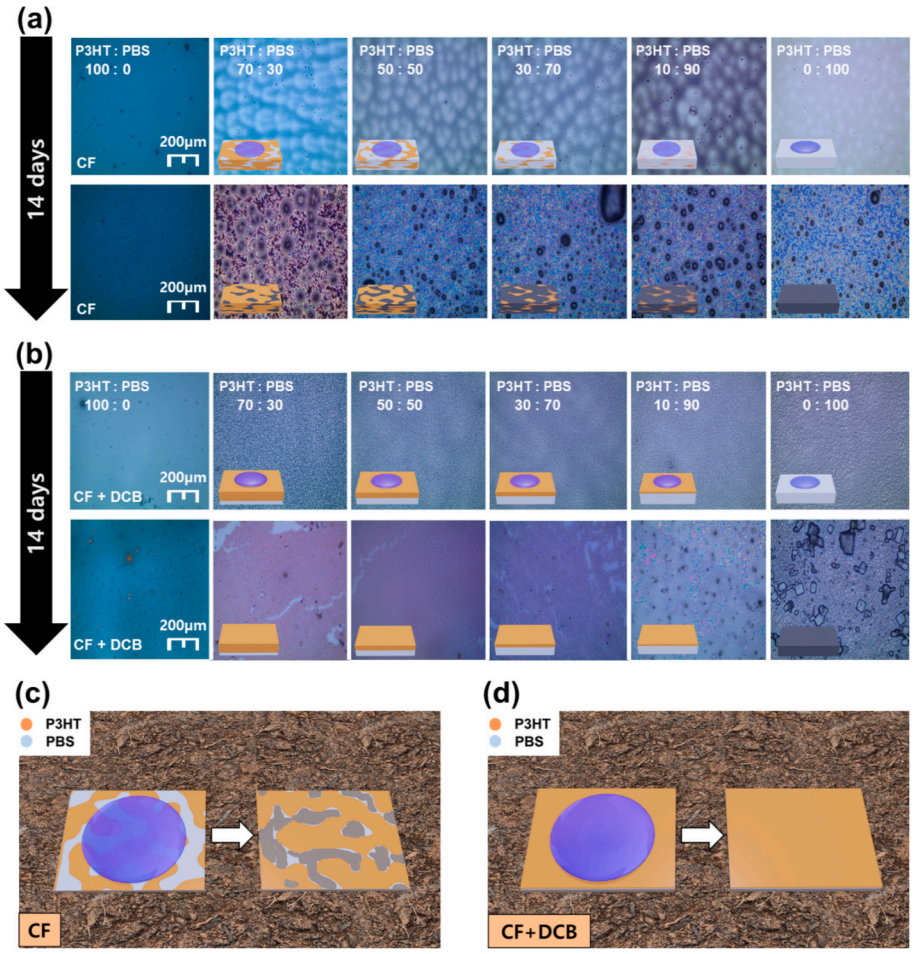

Fig. 7. OM images showing the morphological changes of P3HT/PBS blend films processed with (a) CF and (b) CF:DCB on Si substrates after exposure to seawater for two weeks. Schematic illustrations of the time-dependent biodegradation behavior of P3HT/PBS blend films processed with (c) CF and (d) CF:DCB.

separation, exposing both P3HT and PBS at the top surface. This enabled direct contact between the seawater and PBS domains, thereby promoting the formation of distinct phase-separated structures (Figs. 7a and c). In contrast, the blend films processed with CF:DCB showed vertical phase separation, forming a P3HT-rich top surface layer that limited seawater access to the PBS (Figs. 7b and d).

To further investigate the biodegradation behavior of the P3HT/PBS blended films, they were transferred onto Ecoflex substrates and exposed to seawater. During the inverted transfer process [37], the top surface of the blend film (originally exposed to air) was placed in contact with the Ecoflex substrate, whereas the bottom layer was exposed to air, resulting in an inverted film configuration (Fig. S7). In the blend films processed with CF, partial seawater penetration was observed in the horizontally phase-separated films, which gradually degraded over time. In contrast, the blend films processed with CF:DCB exhibited vertical phase separation, and upon transfer, the PBS-rich bottom layer was exposed on the top surface. This configuration facilitated more uniform and extensive contact with seawater, which showed clear signs of degradation after two weeks. These results indicate the biodegradability of the PBS-blended active layer and show that the degree of degradation depends on the phase-separation configuration.

4. Conclusion

This study systematically investigated the effect of solvent selection on charge transport, sensing performance, flexibility, and biodegradability of gas sensors via the phase separation of P3HT/PBS blend films. CF-processed blend films exhibited horizontal phase separation, which facilitated interactions between gas molecules and ester groups of PBS, thereby contributing to high sensitivity in gas-sensing applications. In contrast, CF:DCB-processed films showed vertical phase separation, forming a P3HT-rich top layer that enabled efficient charge transport and stable electrical performance, even at extremely low P3HT content. In addition, increasing the PBS content improved mechanical flexibility owing to the intrinsic ductility and low glass transition temperature of PBS. Biodegradation studies revealed that both horizontally and vertically phase-separated blend films possess degradation potential in seawater. This study highlights the critical role of solvent engineering in tailoring the multifunctional properties of P3HT/PBS blend films and paves the way for their optimized use in flexible and biodegradable electronic devices.

CRediT authorship contribution statement

Seong Jin Kim: Writing – original draft, Investigation, Formal analysis, Data curation. **Duho Jang:** Investigation, Data curation. **Soyeon An:** Investigation, Formal analysis. **Dong-Ku Kang:** Conceptualization. **Yeong Don Park:** Writing – review & editing, Supervision, Funding acquisition, Conceptualization.

Declaration of competing interest

The authors declare that they have no known competing financial interests or personal relationships that could have appeared to influence the work reported in this paper.

Acknowledgments

This work was supported by an Incheon National University grant in 2025.

Appendix A. Supplementary data

Supplementary data to this article can be found online at https://doi.org/10.1016/j.cej.2025.168910.

Data availability

Data will be made available on request.

References

[1] H. Carvalho, New WHO global air quality guidelines: more pressure on nations to reduce air pollution levels, Lancet Planet. Health 5 (11) (2021) e760–e761, https://doi.org/10.1016/S2542-5196(21)00287-4.
[2] R. Nieder, D.K. Benbi, Reactive nitrogen compounds and their influence on human health: an overview, Rev. Environ. Health 37 (2) (2022) 229–246, https://doi.org/10.1515/reveh-2021-0021.
[3] H. Xu, Y. Jia, Z. Sun, J. Su, Q.S. Liu, Q. Zhou, G. Jiang, Environmental pollution, a hidden culprit for health issues, Eco-Environ. Health 1 (1) (2022) 31–45, https://doi.org/10.1016/j.eehl.2022.04.003.
[4] S.W. Lee, W. Lee, Y. Hong, G. Lee, D.S. Yoon, Recent advances in carbon material-based NO_2 gas sensors, Sensors Actuators B Chem. 255 (2018) 1788–1804, https://doi.org/10.1016/j.snb.2017.08.203.
[5] H.-J. Kim, J.-H. Lee, Highly sensitive and selective gas sensors using p-type oxide semiconductors: overview, Sensors Actuators B Chem. 192 (2014) 607–627, https://doi.org/10.1016/j.snb.2013.11.005.
[6] J. Lee, J.H. Chun, Y. Kim, D. Lee, T.W. Yoon, G. Zhang, W.H. Lee, B. Kang, Ultrasensitive flexible NO_2 sensors with remote-controllable ADC-electropolymerized conducting polymers on plastic, ACS Nano 19 (5) (2025) 5515–5525.
[7] S. Dhall, B.R. Mehta, A.K. Tyagi, K. Sood, A review on environmental gas sensors: materials and technologies, Sens. Int. 2 (2021), https://doi.org/10.1016/j.sintl.2021.100116.
[8] A. Ghouma, B. Salem, S. Cavalaglio, J.-R. Plaussu, G. Crowin, R. Ben Abbes, S. Monfray, T. Fiorido, M. Bendahan, A. Souifi, Near-room-temperature CO_2 capacitive sensors based on hybrid polymer sensitive materials, IEEE Sensors J. 25 (6) (2025) 9331–9340, https://doi.org/10.1109/jsen.2025.3537180.
[9] R. Zhu, J. Gao, Q. Tian, M. Li, Q. Gao, X. Wu, S. Xu, Y. Zhang, Optical chemical gas sensor based on spectral autocorrelation: a method for online detection of nitric oxide and ammonia in exhaled breath, Sensors Actuators B Chem. 422 (2025), https://doi.org/10.1016/j.snb.2024.136694.
[10] J. Shintake, Y. Piskarev, S.H. Jeong, D. Floreano, Ultrastretchable strain sensors using carbon black-filled elastomer composites and comparison of capacitive versus resistive sensors, Adv. Mater. Technol. 3 (3) (2017), https://doi.org/10.1002/admt.201700284.
[11] T. Dong, Y. Gu, T. Liu, M. Pecht, Resistive and capacitive strain sensors based on customized compliant electrode: comparison and their wearable applications, Sensors Actuators A 326 (2021), https://doi.org/10.1016/j.sna.2021.112720.
[12] M. Zammali, S. Liu, W. Yu, A Flexible, Transparent, Ultralow detection limit capacitive pressure sensor, Adv. Mater. Interfaces 9 (17) (2022), https://doi.org/10.1002/admi.202200015.
[13] S. Hong, M. Wu, Y. Hong, Y. Jeong, G. Jung, W. Shin, J. Park, D. Kim, D. Jang, J.-H. Lee, FET-type gas sensors: a review, Sensors Actuators B Chem. 330 (2021), https://doi.org/10.1016/j.snb.2020.129240.
[14] G. Lu, T. Ji, S. He, F. Ai, L. Yan, J. Hu, Recent progress of exhaled gas-based diagnosis based on field effect transistor sensors, Adv. Funct. Mater. 35 (21) (2024), https://doi.org/10.1002/adfm.202309111.
[15] I.H. Ko, Y.D. Park, Recent research trends for developing highly sensitive, flexible organic field-effect transistor-based gas sensors, ACS Appl. Polym. Mater. 7 (5) (2025) 2749–2760, https://doi.org/10.1021/acsapm.4c03902.
[16] Z. Zhang, B. Cheng, Y. Zhang, Room-temperature operable, fully recoverable ethylene gas sensor via pulsed electric field modulation, Adv. Sci. 12 (19) (2025) e2500389, https://doi.org/10.1002/advs.202500389.
[17] R. Sultana, S. Wang, M.S. Abbasi, K.A. Shah, M. Mubeen, L. Yang, Q. Zhang, Z. Li, Y. Han, Enhancing sensitivity, selectivity, and intelligence of gas detection based on field-effect transistors: principle, process, and materials, J. Environ. Sci. 154 (2025) 174–199, https://doi.org/10.1016/j.jes.2024.07.027.
[18] C. Zhang, P. Chen, W. Hu, Organic field-effect transistor-based gas sensors, Chem. Soc. Rev. 44 (8) (2015) 2087–2107, https://doi.org/10.1039/c4cs00326h.
[19] S. Zhang, Y. Zhao, X. Du, Y. Chu, S. Zhang, J. Huang, Gas sensors based on nano/microstructured organic field-effect transistors, Small 15 (12) (2019) e1805196, https://doi.org/10.1002/smll.201805196.
[20] P. Nie, H. Wu, X. Maimaitiyiming, Polycarbazole-based polymer/semiconductor carbon nanotube composites for NO_2 and NH_3 gas sensing applications, Sep. Purif. Technol. 363 (2025), https://doi.org/10.1016/j.seppur.2025.132038.
[21] J.F. Martinez Hardigree, H.E. Katz, Through thick and thin: tuning the threshold voltage in organic field-effect transistors, Acc. Chem. Res. 47 (4) (2014) 1369–1377, https://doi.org/10.1021/ar5000049.
[22] Z. Wang, P.K. Nayak, J.A. Caraveo-Frescas, H.N. Alshareef, Recent developments in p-type oxide semiconductor materials and devices, Adv. Mater. 28 (20) (2016) 3831–3892, https://doi.org/10.1002/adma.201503080.
[23] P. Ding, D. Yang, S. Yang, Z. Ge, Stability of organic solar cells: toward commercial applications, Chem. Soc. Rev. 53 (5) (2024) 2350–2387, https://doi.org/10.1039/d3cs00492a.
[24] X. He, Z. Zhong, Y. Ouyang, J. Wang, Investigation of tribo-electrostatic separation mechanism for thermoplastics in e-waste based on functional group distribution and surface potential, Sep. Purif. Technol. 362 (2025), https://doi.org/10.1016/j.seppur.2025.131764.
[25] A. Kumar, G. Anjum, J.N. Moorthy, Design and synthesis of tetralactam macrocycle-based porous organic polymers (POPs): application in the recovery of gold from e-waste, RSC Appl. Polym. 3 (3) (2025) 603–612, https://doi.org/10.1039/d4lp00218k.
[26] S.H. Kim, W.M. Yoon, M. Jang, H. Yang, J.-J. Park, C.E. Park, Damage-free hybrid encapsulation of organic field-effect transistors to reduce environmental instability, J. Mater. Chem. 22 (16) (2012), https://doi.org/10.1039/c2jm13329f.
[27] L. Manfra, V. Marengo, G. Libralato, M. Costantini, F. De Falco, M. Cocca, Biodegradable polymers: a real opportunity to solve marine plastic pollution? J. Hazard. Mater. 416 (2021) 125763 https://doi.org/10.1016/j.jhazmat.2021.125763.
[28] A. Nakayama, N. Yamano, N. Kawasaki, Biodegradation in seawater of aliphatic polyesters, Polym. Degrad. Stab. 166 (2019) 290–299, https://doi.org/10.1016/j.polymdegradstab. 2019.06.006.
[29] Y. Muranaka, T. Koike, T. Osuga, T. Maki, Degradation behavior of polybutylene succinate with fillers, Polym. Degrad. Stab. 235 (2025), https://doi.org/10.1016/j.polymdegradstab. 2025.111266.
[30] J.F. Kim, H.J. Kim, J. Park, H. Jeon, J.G. Kim, C. Choi, K.-H. Nam, G. Shin, S. H. Park, J. Shin, D.-K. Kang, D.X. Oh, D.Y. Lee, S.W. Hong, G.-R. Yi, Research roadmap for sustainable polymeric materials in Korea, Macromol. Res. 33 (5) (2025) 535–551, https://doi.org/10.1007/s13233-024-00357-4.
[31] G.W. Kim, Y.J. Jang, M. Kim, Y.D. Park, Floating-non-solvent method for inducing the formation of highly crystalline conjugated polymer nanofibrils in the solution state for high-performance organic transistors, J. Mater. Chem. C 6 (31) (2018) 8353–8359, https://doi.org/10.1039/c8tc01525b.
[32] K.A. Larasati, C. Park, L. Ayuningtias, H. Cha, Y.-H. Kim, Side chain effect of benzodithiophene on the diketopyrrolopyrrole-based copolymer for the opto-electronic properties, Macromol. Res. (2025), https://doi.org/10.1007/s13233-025-00394-7.
[33] D. Jang, S.Y. Park, H.S. Lee, Y.D. Park, Low-regioregularity polythiophene for a highly sensitive and stretchable gas sensor, ACS Appl. Mater. Interfaces 15 (27) (2023) 32629–32636, https://doi.org/10.1021/acsami.3c05278.
[34] E.H. Kwon, Y.J. Jang, G.W. Kim, M. Kim, Y.D. Park, Highly crystalline and uniform conjugated polymer thin films by a water-based biphasic dip-coating technique minimizing the use of halogenated solvents for transistor applications, RSC Adv. 9 (11) (2019) 6356–6362, https://doi.org/10.1039/c8ra09231a.
[35] G. Zhang, W. Zhou, M. Kim, M. Sun, H. Lu, L. Qiu, K. Cho, Y. Ding, Acceptor–donor–acceptor molecule processed using polar non-halogenated solvents for organic field-effect transistors, J. Mater. Chem. C 8 (19) (2020) 6496–6502, https://doi.org/10.1039/c9tc07117b.
[36] E.H. Kwon, G.W. Kim, M. Kim, Y.D. Park, Effect of alcohol polarity on the aggregation and film-forming behaviors of poly(3-hexylthiophene), ACS Appl. Polym. Mater. 2 (7) (2020) 2980–2986, https://doi.org/10.1021/acsapm.0c00448.
[37] I.H. Ko, S.Y. Park, Y.D. Park, Controlling the molecular weight of poly(3-hexylthiophene) for highly sensitive and flexible gas sensor, Sensors Actuators B Chem. 433 (2025), https://doi.org/10.1016/j.snb.2025.137554.
[38] J. Zuo, T. Jin, H. Li, J. Li, X. Liu, X. Yu, Y. Han, Y. Han, Continuous conjugated polymer network in elastomer matrix arising from solution-state aggregation and film-forming dynamics favoring mechanical and electrical properties, Adv. Funct. Mater. (2025), https://doi.org/10.1002/adfm.202424785.
[39] L. Qiu, W.H. Lee, X. Wang, J.S. Kim, J.A. Lim, D. Kwak, S. Lee, K. Cho, Organic thin-film transistors based on polythiophene nanowires embedded in insulating polymer, Adv. Mater. 21 (13) (2009) 1349–1353, https://doi.org/10.1002/adma.200802880.
[40] H.-C. Hsieh, N. Wu, T.-H. Chuang, W.-Y. Lee, J.-Y. Chen, W.-C. Chen, Eco-friendly polyfluorene/poly(butylene succinate) blends and their electronic device application on biodegradable substrates, ACS Appl. Polym. Mater. 2 (6) (2020) 2469–2476, https://doi.org/10.1021/acsapm.0c00439.
[41] Q. Liang, Z. Miao, X. Liu, Z. Liu, Z. Xu, Y. Zhang, Z. Zhang, W. Zhai, C. Song, J. Xin, X. Yin, J. Liu, The phase separation control in all-polymer solar cells, SusMat 5 (3) (2025), https://doi.org/10.1002/sus2.70003.
[42] L. Qiu, J.A. Lim, X. Wang, W.H. Lee, M. Hwang, K. Cho, Versatile use of vertical-phase-separation-induced bilayer structures in organic thin-film transistors, Adv. Mater. 20 (6) (2008) 1141–1145, https://doi.org/10.1002/adma.200702505.
[43] S. Hou, J. Yu, X. Zhuang, D. Li, Y. Liu, Z. Gao, T. Sun, F. Wang, X. Yu, Phase separation of P3HT/PMMA blend film for forming semiconducting and dielectric layers in organic thin-film transistors for high-sensitivity NO_2 detection, ACS Appl. Mater. Interfaces 11 (47) (2019) 44521–44527, https://doi.org/10.1021/acsami.9b15651.
[44] L. Zhang, X. Xing, L. Zheng, Z. Chen, L. Xiao, B. Qu, Q. Gong, Vertical phase separation in bulk heterojunction solar cells formed by in situ polymerization of fulleride, Sci. Rep. 4 (2014) 5071, https://doi.org/10.1038/srep05071.

[45] X. Guo, L. Liu, Z. Zhuang, X. Chen, M. Ni, Y. Li, Y. Cui, P. Zhan, C. Yuan, H. Ge, Z. Wang, Y. Chen, A new strategy of lithography based on phase separation of polymer blends, Sci. Rep. 5 (2015) 15947, https://doi.org/10.1038/srep15947.
[46] A. Bleiziffer, F. Deussen, J. Rühe, Durable anti-fogging polymer coatings based on C,H insertion cross–linking (CHic) that are user and environmentally friendly, Adv. Mater. Technol. (2025), https://doi.org/10.1002/admt.202500276.
[47] E. Bogdanova, M. Liu, P. Hodapp, A. Borbora, W. Wenzel, S. Brase, A. Jung, Z. Dong, P.A. Levkin, U. Manna, T. Hashem, C. Woll, Functionalization of monolithic MOF thin films with hydrocarbon chains to achieve superhydrophobic surfaces with tunable water adhesion strength, Mater. Horiz. 12 (4) (2025) 1274–1281, https://doi.org/10.1039/d4mh00899e.
[48] Y. Liu, Z. Yin, C. Liu, Z. Liu, S. Liu, Q. Zheng, Photo-crosslinked polymer dielectrics enabling flexible organic transistor synapses with excellent linearity for neuromorphic applications, Chem. Eng. J. 507 (2025), https://doi.org/10.1016/j.cej.2025.160538.
[49] A. Kozbial, Z. Li, C. Conaway, R. McGinley, S. Dhingra, V. Vahdat, F. Zhou, B. D'Urso, H. Liu, L. Li, Study on the surface energy of graphene by contact angle measurements, Langmuir 30 (28) (2014) 8598–8606, https://doi.org/10.1021/la5018328.
[50] Z. Wei, J. Gu, Y. Ye, M. Fang, J. Lang, D. Yang, Z. Pan, Biodegradable poly (butylene succinate) nanofibrous membrane treated with oxygen plasma for superhydrophilicity, Surf. Coat. Technol. 381 (2020), https://doi.org/10.1016/j.surfcoat.2019.125147.
[51] A. Motta, G. Seguini, M. Perego, R. Consonni, A.C. Boccia, G. Ambrosio, C. Baratto, P. Cerruti, M. Lavorgna, S. Tagliabue, C. Wiemer, Sequential infiltration synthesis of Al_2O_3 in biodegradable polybutylene succinate: characterization of the infiltration mechanism, ACS Appl. Polym. Mater. 4 (10) (2022) 7191–7203, https://doi.org/10.1021/acsapm.2c01073.
[52] D. Jang, H. Jin, M. Kim, Y.D. Park, Polymeric interfacial engineering approach to perovskite-functionalized organic transistor-type gas sensors, Chem. Eng. J. 473 (2023), https://doi.org/10.1016/j.cej.2023.145482.
[53] T.D. Tsai, J.W. Chang, T.C. Wen, T.F. Guo, Manipulating the hysteresis in poly (vinyl alcohol)-dielectric organic field-effect transistors toward memory elements, Adv. Funct. Mater. 23 (34) (2013) 4206–4214, https://doi.org/10.1002/adfm.201203694.
[54] Y.D. Park, J.A. Lim, H.S. Lee, K. Cho, Interface engineering in organic transistors, Mater. Today 10 (3) (2007) 46–54, https://doi.org/10.1016/s1369-7021(07)70019-6.
[55] H. Qu, Z. Zhuo, X. Zhao, S. Zhang, X. Ma, Y. Zou, K. Yang, F. Zhang, Organic thin film transistor material based photomultiplication type organic photodetectors via balancing hole tunneling injection and transport, Adv. Opt. Mater. (2025), https://doi.org/10.1002/adom.202501632.
[56] H.-J. Tai, Dielectric spectroscopy of poly(butylene succinate) films, Polymer 48 (15) (2007) 4558–4566, https://doi.org/10.1016/j.polymer.2007.05.043.
[57] L. Yu, Y. Zhang, W. Tong, J. Shang, B. Shen, F. Lv, P.K. Chu, Green dielectric materials composed of natural graphite minerals and biodegradable polymer, RSC Adv. 2 (23) (2012), https://doi.org/10.1039/c2ra20956j.
[58] J.B. Clark, H.C. Allen, Interfacial carbonyl groups of propylene carbonate facilitate the reversible binding of nitrogen dioxide, Phys. Chem. Chem. Phys. 26 (21) (2024) 15733–15741, https://doi.org/10.1039/d4cp01382d.
[59] M. Hong, P.U. Do, C.H. Lee, Y.D. Park, Harnessing the potential of porous carbon derived from chlorinated polyvinyl chloride as an effective gas analyte channel for NO_2 organic sensors, Sensors Actuators B Chem. 421 (2024), https://doi.org/10.1016/j.snb.2024.136463.
[60] B. King, B.H. Lessard, Review of recent advances and sensing mechanisms in solid-state organic thin-film transistor (OTFT) sensors, J. Mater. Chem. C 12 (16) (2024) 5654–5683, https://doi.org/10.1039/d3tc03611a.
[61] S.J. Park, J.Y. Kim, D.H. Kim, D. Jang, Y.D. Park, Additive engineering for high-performance polythiophene gas sensors incorporating functional amine additive with strong binding energy for NO_2, J. Mater. Chem. C 12 (27) (2024) 9986–9992, https://doi.org/10.1039/d4tc01356e.
[62] M. Hong, P.U. Do, C.H. Lee, Y.D. Park, Enhanced gas sensing performance of polythiophene film with surface engineered porous carbon, Appl. Surf. Sci. 692 (2025), https://doi.org/10.1016/j.apsusc.2025.162679.
[63] B. Petrovic, M. Gorbounov, S. Masoudi Soltani, Impact of surface functional groups and their introduction methods on the mechanisms of CO_2 adsorption on porous carbonaceous adsorbents, Carbon Capture Sci. Technol. 3 (2022), https://doi.org/10.1016/j.ccst.2022.100045.
[64] M. Shaik, V.K. Rao, A.K. Sinha, K.S.R.C. Murthy, R. Jain, Sensitive detection of nitrogen dioxide gas at room temperature using poly(3,4-ethylenedioxythiophene) nanotubes, J. Environ. Chem. Eng. 3 (3) (2015) 1947–1952, https://doi.org/10.1016/j.jece.2015.07.001.
[65] M.A. Chougule, D.S. Dalavi, S. Mali, P.S. Patil, A.V. Moholkar, G.L. Agawane, J. H. Kim, S. Sen, V.B. Patil, Novel method for fabrication of room temperature polypyrrole–ZnO nanocomposite NO2 sensor, Measurement 45 (8) (2012) 1989–1996, https://doi.org/10.1016/j.measurement.2012.04.023.
[66] L. Malepe, D.T. Ndinteh, P. Ndungu, M.A. Mamo, The detection of volatile organic compounds using a CNPs/polypyrrole-based solid-state sensor operating at room temperature, Mater. Chem. Phys. 332 (2025), https://doi.org/10.1016/j.matchemphys.2024.130186.
[67] Z. Wang, L. Huang, X. Zhu, X. Zhou, L. Chi, An ultrasensitive organic semiconductor NO2 sensor based on crystalline TIPS-pentacene films, Adv. Mater. 29 (38) (2017), https://doi.org/10.1002/adma.201703192.
[68] M. Hong, S.Y. Park, J.E. Lee, Y.D. Park, High-performance flexible organic gas sensor via alkyl side chain engineering of polyalkylthiophene, Chem. Eng. J. 480 (2024), https://doi.org/10.1016/j.cej.2023.147962.
[69] Y.R. Choi, Y.-G. Yoon, K.S. Choi, J.H. Kang, Y.-S. Shim, Y.H. Kim, H.J. Chang, J.-H. Lee, C.R. Park, S.Y. Kim, H.W. Jang, Role of oxygen functional groups in graphene oxide for reversible room-temperature NO_2 sensing, Carbon 91 (2015) 178–187, https://doi.org/10.1016/j.carbon.2015.04.082.
[70] D.K. Hwang, C. Fuentes-Hernandez, J.B. Kim, W.J. Potscavage, B. Kippelen, Flexible and stable solution-processed organic field-effect transistors, Org. Electron. 12 (7) (2011) 1108–1113, https://doi.org/10.1016/j.orgel.2011.04.002.
[71] A. Vilouras, A. Christou, L. Manjakkal, R. Dahiya, Ultrathin ion-sensitive field-effect transistor chips with bending-induced performance enhancement, ACS Appl. Electron. Mater. 2 (8) (2020) 2601–2610, https://doi.org/10.1021/acsaelm.0c00489.
[72] S.B. Park, H. Kwak, D. Lee, G. Shin, M. Jang, H. Jung, H. Jeon, H.J. Kim, J. Park, D. X. Oh, Development of marine-degradable poly(ester amide)s with strong, up-scalable, and up-cyclable performance, Adv. Mater. 37 (9) (2025) e2417266, https://doi.org/10.1002/adma.202417266.